OPTIMIZATION OF STELLARATOR REACTOR PARAMETERS

J. F. Lyon[1], L.P. Ku[2], P. Garabedian[3], L. El-Guebaly[4], L. Bromberg[5], and the ARIES Team

[1]*Oak Ridge National Laboratory, Oak Ridge, TN, lyonjf@ornl.gov*
[2]*Princeton Plasma Physics Laboratory, Princeton, NJ, lpku@pppl.gov*
[3]*New York University, New York, NY, garabedian@cims.nyu.edu*
[4]*University of Wisconsin, Madison, WI, elguebaly@engr.wisc.edu*
[5]*Massachusetts Inst. of Technology, Cambridge, MA, brom@psfc.mit.edu*

Four quasi-axisymmetric compact stellarator plasma and coil configurations are analyzed for their potential as reactors. A 0-D (volume-average) approach for optimizing the main reactor parameters allows study of the relationship between global parameters and the compatibility of different constraints for a given power output including plasma-coil spacing, coil-coil spacing, maximum field and coil current density, neutron wall loading, plasma beta value, etc. The result is reactor candidates with average major radii <R> in the 6-7 m range, a factor of two smaller than those of previous studies. A 1-D power balance code is used to study the ignited operating point and the effect of different plasma and confinement assumptions including density and temperature profiles, alpha particle losses, and helium particle confinement time for the different plasma and coil configurations.

I. COMPACT STELLARATORS

Compact stellarators[1] are low-aspect-ratio stellarator-tokamak hybrids with the potential for an attractive, fully ignited reactor. Because the confining poloidal magnetic field is created by currents in external windings aided by a modest plasma bootstrap current, compact stellarators are inherently steady-state devices without the large plasma current of the tokamak and spherical torus approaches. Compact stellarators may combine the best features of high-current tokamaks (moderate plasma aspect ratios, good confinement, and high volume-average plasma beta $\langle\beta\rangle$) with those of large-aspect-ratio currentless stellarators (steady-state operation without external current drive or disruptions, stability against external kinks and vertical displacement events without a close conducting wall or active feedback systems, and low recirculating power in a reactor). However, earlier stellarator power plant studies led to large reactor sizes. The German HSR reactor study[2] had an average major radius $\langle R\rangle$ = 22 m in the five-field-period (M = 5) embodiment and $\langle R\rangle$ = 18 m in a more recent M = 4 version. The M = 4 ARIES Stellarator Power Plant Study (SPPS) reactor[3], with $\langle R\rangle$ = 14 m arising from its larger plasma-coil spacing compared to other stellarators, was a first step toward a smaller-size reactor. The SPPS reactor with its higher wall power density and low recirculating power was calculated to be cost competitive[4] with the R = 6 m ARIES-IV and R = 5.5 m ARIES-RS tokamak reactors. A more compact stellarator reactor should retain the cost savings associated with the low recirculating power of the SPPS reactor, but with smaller size and higher wall power density (hence lower cost of electricity) by taking advantage of newly developed plasma and coil configurations and an improved blanket and shield concept[5]. Three tools have been developed to optimize the main reactor parameters ($\langle R\rangle$, the average magnetic field on axis $\langle B_{axis}\rangle$, etc.): a 0-D code to study the relationship between global parameters, a 1-D power balance code, and a 1-D reactor systems/optimization code to optimize the reactor parameters for minimum cost of electricity. The first two are discussed here; the third is the subject of a separate paper.

Four compact stellarator configurations have been analyzed: an M = 3 NCSX-based[6] plasma configuration with two different modular coil sets (NCSX-1, -2) and 8-coil and 16-coil versions of an M = 2 plasma configuration[7] (MHH2-8, -16). Figure 1 shows top views of the plasma and nonplanar modular coils for the NCSX-1 and MHH2-8 configurations. As with other stellarators, the plasma is non-axisymmetric with a noncircular cross section, which is needed to create the required rotational transform ($\iota = 1/q$, where q is the tokamak safety factor) without a large toroidal plasma current. However, the compact stellarator variant studied is quasi-toroidally symmetric[8]; the strength of the magnetic field $|\boldsymbol{B}|$ varies little in the toroidal coordinate direction in magnetic field line coordinates, analogous to the axisymmetry of $|\boldsymbol{B}|$ in tokamaks, spherical tori and reverse field pinches. To create the necessary poloidal field from external coils, the coils must be nonplanar with large toroidal excursions and bends with small radii of curvature. The NCSX-1 and NCSX-2 coil configurations have the same plasma geometry but different coil configurations; NCSX-2 has a smaller plasma-coil separation Δ for a given $\langle R\rangle$. The MHH2-8 and MHH2-16 configurations have different plasma aspect ratios, number of modular coils, and coil geometries. For those configurations the coils are closer to the plasma on the outboard side and have less toroidal excursion than the NCSX-1, -2 coils. Thus the region where $\Delta < \Delta_{min}$ + 0.2 m occurs over a larger area and a

full blanket and shield is required everywhere. The plasma-coil spacings for the NCSX-1, -2 configurations allow sector (end) or port (radial) maintenance while the MHH2 configurations require maintenance through ports.

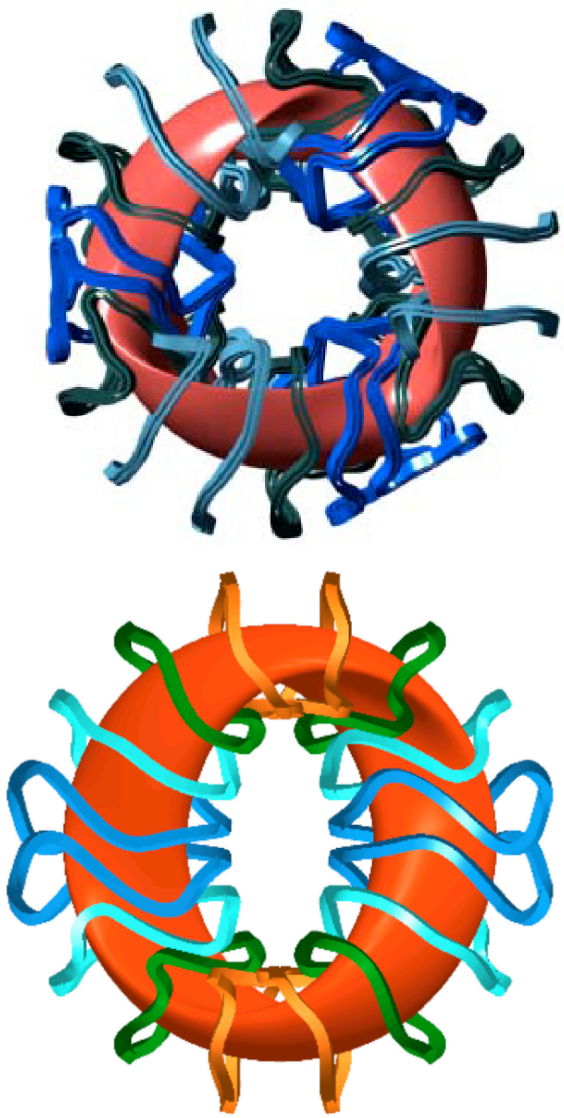

Fig. 1. Two compact stellarator plasma and coil configurations: NCSX-1 (top) and MHH2-16 (bottom).

Determination of the reactor parameters involves both the plasma and coil geometry and the reactor constraints. The plasma geometry enters through the shape of the last closed flux surface and the coil geometry enters through the shape of the modular coils. Stellarator plasma and coil configurations can be characterized by a number of dimensionless parameters. Table I lists these parameters for the four configurations that were studied:

* the plasma aspect ratio $A_p = \langle R\rangle/\langle a\rangle$ where $\langle a\rangle$ is the average radius of the non-circular and non-axisymmetric stellarator plasma,
* $A_{surf}/\langle R\rangle^2$ where A_{surf} is the area of the last closed flux surface,
* $A_{\square} = \langle R\rangle/\square_{min}$ where $\square_{min}$ is the minimum distance between the edge of the plasma and the current center of the modular coil winding pack,
* $A_{c\text{-}c,min} = \langle R\rangle/d_{coil\text{-}coil}$ where $d_{coil\text{-}coil}$ is the minimum distance between two modular coils,
* L_{coil} is the total length of all the coils in the modular coil set, and
* $B_{max}/\langle B_{axis}\rangle$ is a function of d and k where B_{max} is the maximum field on the modular coil winding pack, d^2 is the cross sectional area of the winding pack, and k is the toroidal elongation of the winding pack; the entries in Table I are for $d = 0.4$ m and $k = 1$.

TABLE I. Geometrical Properties of Four Compact Stellarator Reactor Candidates.

Configuration Properties	NCSX-1	NCSX-2	MHH2-8	MHH2-16
A_p	4.50	4.50	2.70	3.75
$A_{surf}/\langle R\rangle^2$	11.80	11.95	19.01	13.37
$A_{\square}$	5.90	6.88	4.91	5.52
$A_{c\text{-}c,min}$	10.07	9.38	7.63	13.27
$L_{coil}/\langle R\rangle$	89.7	88.3	44.1	64.6
$B_{max}/\langle B_{axis}\rangle$	2.10	1.84	3.88	2.77

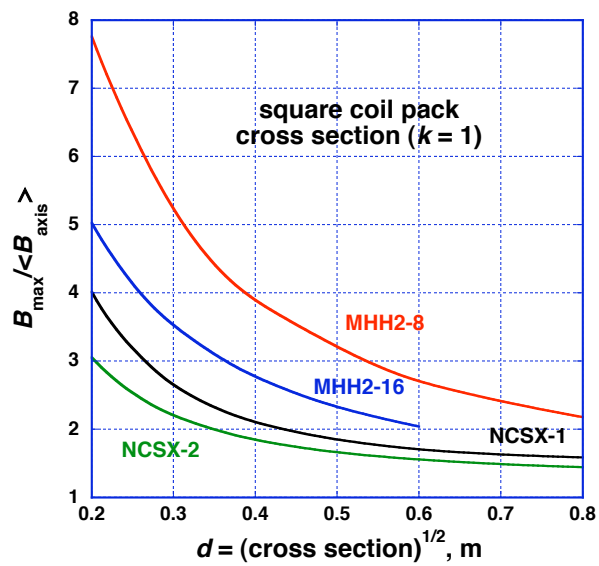

Fig. 2. Variation of $B_{max}/\langle B_{axis}\rangle$ with coil pack size.

Most of the device parameters depend algebraically on $\langle R\rangle$, but B_{max} and d must be determined from both $\langle R\rangle$ and the $B_{max}/\langle B_{axis}\rangle$ ratio calculated for finite-size coil cross sections. Figure 2 shows the dependence of $B_{max}/\langle B_{axis}\rangle$ on d for a square coil pack ($k = 1$) and initial reference values of $\langle R\rangle$ for the four configurations considered here. The large variation in $B_{max}/\langle B_{axis}\rangle$ for a

given d arises from the differences in $A_{\square}$ shown in Table I, which reflects the increasing complexity (higher spatial harmonic content) of the coils as $\square/\langle R\rangle$ increases. A higher spatial harmonic content is required to create a desired magnetic field spectrum at the plasma surface as the plasma-coil distance increases ($A_{\square}$ decreases) because the higher spatial harmonics of the magnetic field from the coils decay faster with distance from the coils. NCSX-2 has a smaller plasma-coil separation for a given $\langle R\rangle$ than NCSX-1, and consequently a smaller $B_{max}/\langle B_{axis}\rangle$. The MHH2-8 configuration has the largest $A_{\square}$ and hence the largest $B_{max}/\langle B_{axis}\rangle$ for a given $\langle R\rangle$. Stellarator coil configurations with a smaller plasma-coil distance for a given $\langle R\rangle$ lead to larger reactors because of the relatively fixed distance needed for the first wall, blanket, shield, vacuum vessel, coil structure and assembly gaps; coil configurations with a larger plasma-coil distance for a given $\langle R\rangle$ (smaller $A_{\square}$) have more convoluted coils and higher $B_{max}/\langle B_{axis}\rangle$, which reduces the maximum $\langle B_{axis}\rangle$ for an allowable B_{max}. The value of $B_{max}/\langle B_{axis}\rangle$ also depends on the value of k, as shown in Fig. 3 where it is normalized to its value for $k = 1$. In this study the value of $k = k_{max}$ is chosen such that there is only a 2-cm gap between coils toroidally where two coils are closest to each other. For each coil configuration, the value of k_{max} depends on $\langle R\rangle$ and d. Typical k_{max} values range from 1.9 to 5 for the configurations of interest.

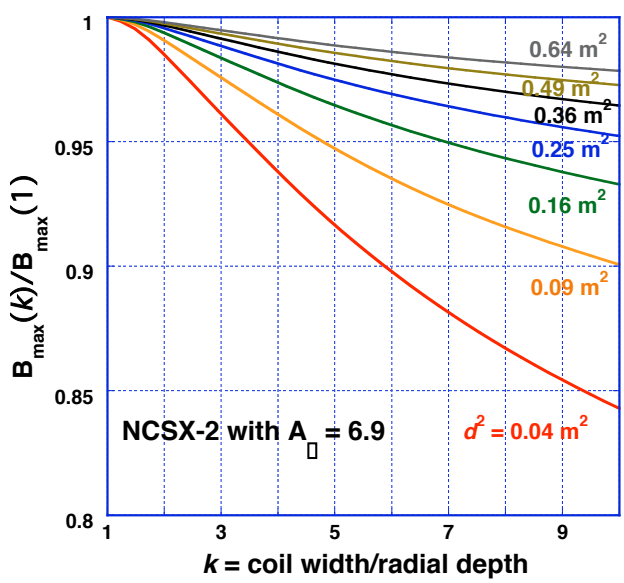

Fig. 3. Variation of B_{max} with toroidal coil elongation.

II. 0-D OPTIMIZATION

A 0-D (volume-average) approach for optimizing the main reactor parameters allows study of the relationship between global parameters and the compatibility of different constraints for a given power output: the plasma-coil spacing, coil-coil spacing, B_{max} and coil current density j_{coil}, maximum neutron wall loading $p_{n,max}$, $\square/\square$ etc. For each coil configuration a given average neutron wall loading $\langle p_{n,wall}\rangle$ uniquely determines $\langle R\rangle$ through the $A_{surf}/\langle R\rangle^2$ parameter, the value of P_{fusion}, and calculations[9] that give $\langle p_{n,wall}\rangle = p_{n,max}/1.5$. Fixing the allowable value for $\square/\square$ then determines the value of $\langle B_{axis}\rangle \sim \square^{1/2}\langle R\rangle^{-3/4}$ through the expression for P_{fusion} ($\sim \square^2\langle B_{axis}\rangle^4\langle R\rangle^3$) and gives the necessary energy confinement time $\square_E \sim \square\langle B_{axis}\rangle^2/P_{fusion} \sim 1/(\square\langle B_{axis}\rangle^2\langle R\rangle^3)$. However, the results are constrained by the requirements that there be (1) adequate distance between the edge of the plasma and the center of the nonplanar coils for the plasma scrapeoff region, the first wall, the blanket and shield, the vacuum vessel (if not outside the coils), the coil case, half the radial depth of the coils ($cd/2$), and assembly gaps, and (2) j_{coil} not exceed the current density limit for the low-T_c superconductor, $j_{SC}(B_{max})$. The j_{SC} vs B_{max} curve is based on thin-filament react-and-wind Nb_3Sn superconductor in a cable-in-conduit configuration. The current density is averaged over the conductor, stabilizer, internal structure and helium cooling channels in the coil winding pack. Other options will also be assessed in the next stage of the study. The required thickness t of the blanket and shielding is determined by neutron shielding calculations[5] for each type of blanket and shield. For the LiPb/ferritic steel/He-cooled blanket/shield approach with the vacuum vessel between the shield and the coil case, t(m) = 1.06 + 0.0624 $ln(\langle p_{n,wall}\rangle)$ for the full blanket and shield. If the tritium-breeding blanket can be omitted in a small region of the wall where $\square < \square_{min}$ + 0.2 m, then t can be 0.2 m smaller (allowable for the NCSX-1, -2 cases but not for the MHH2-8, -16 cases). Evaluation of $cd = d/k^{1/2}$ and incorporation of the $j_{coil} \sim \langle B_{axis}\rangle\langle R\rangle/d^2 \sim \langle R\rangle^{1/4}/d^2$ constraint is more complicated because of the $B_{max}/\langle B_{axis}\rangle$

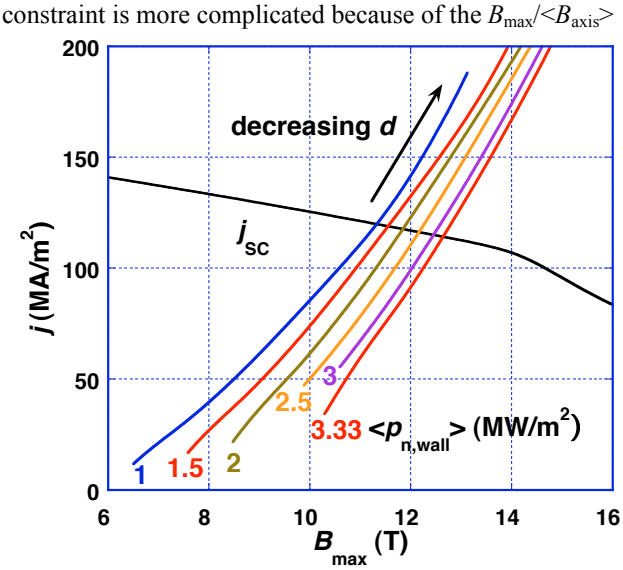

Fig. 4. Determination of j_{coil} and B_{max}.

constraint is more complicated because of the $B_{max}/\langle B_{axis}\rangle$ dependence on d and k in Figs. 2 and 3. The values for B_{max} and d are determined for each $\langle p_{n,wall}\rangle$ from the intersection of the corresponding $j_{coil}(B_{max})$ curve and the $j_{SC}(B_{max})$ curve, as shown in Fig. 4. For the NCSX-1 case the resulting B_{max} varies by only 10% and j_{coil} is approximately constant, varying by only 4%, for a factor of 3 variation in $\langle p_{n,wall}\rangle$. The value of d varies along the j_{coil} curves; the lower end corresponds to d = 0.8 m, a large coil winding pack.

The variation of $\langle R\rangle$ and $\langle B_{axis}\rangle$ with $\langle p_{n,wall}\rangle$ is shown in Fig. 5 for the NCSX-1 case with P_{fusion} = 2 GW (1 $GW_{electric}$ for the assumed 50% thermal conversion efficiency based on an advanced Brayton cycle), □ = 6%, and a 7-cm plasma-wall (scrapeoff) distance. The □ = 6% value is chosen because compact stellarators have high equilibrium beta values and good stability against external kinks and vertical displacement events. Present experiments exceed theoretical beta limits for stellarators and show evidence for a second stability region at higher beta. The no-blanket and full-blanket limit curves are also shown in Fig. 5. A gap exists between the vacuum vessel and the coils because the $\langle R\rangle$ curve lies above the no-blanket limit for the NCSX-1 case and the maximum value for $\langle p_{n,wall}\rangle$ is limited to 3.3 MW/m^2 ($p_{n,max}$ = 5 MW/m^2). The other cases have a lower allowed value for $\langle p_{n,wall}\rangle$ because the NCSX-2 case is limited by the no-blanket curve and the MHH2-8, -16 cases are limited by the full-blanket curve. The optimum value for $\langle p_{n,wall}\rangle$ (~ 1/wall area), and hence for $\langle R\rangle \sim 1/\langle p_{n,wall}\rangle^{0.5}$, is a cost optimization issue that needs to be folded in with other considerations in a systems/optimization code. The capital cost of the modular coils (~ coil volume ~ $L_{coil}I_{coil}/j_{coil}$) varies as $1/\langle p_{n,wall}\rangle^{0.6}$ while that of the first wall, blanket, shielding, and coil structure varies as

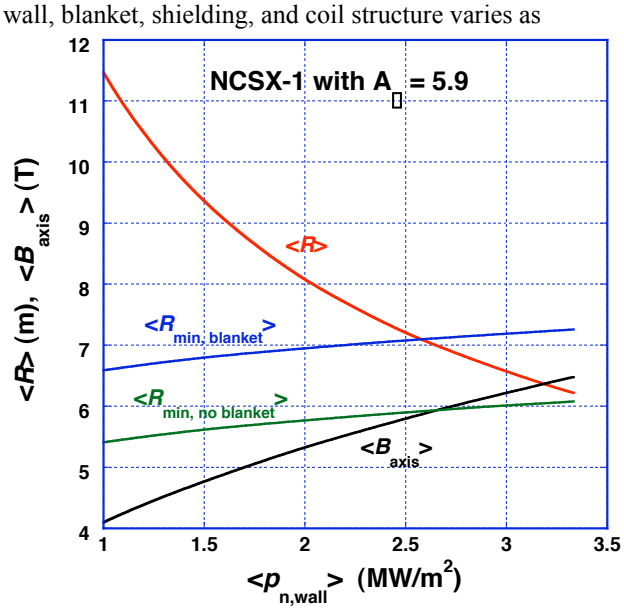

Fig. 5. Variation of $\langle R\rangle$ and $\langle B_{axis}\rangle$ with $\langle p_{n,wall}\rangle$.

$1/\langle p_{n,wall}\rangle$ because the volumes (and costs) of these components are approximately proportional to the wall area (~ $1/\langle p_{n,wall}\rangle$) times a fixed thickness. The cost of replacing the blanket during the reactor lifetime is approximately independent of $\langle p_{n,wall}\rangle$ because the number of times the blanket must be replaced varies as $\langle p_{n,wall}\rangle$ while the cost of the blanket varies as $1/\langle p_{n,wall}\rangle$. These considerations favor a high value for $\langle p_{n,wall}\rangle$.

Table II gives the results obtained with this approach assuming the maximum allowed value for $\langle p_{n,wall}\rangle$ for the four coil configurations. The base assumptions are $P_{electric}$ = 1 GW (P_{fusion} = 2 GW) and □ = 6%. The units in Table II are MW/m^2 for $\langle p_{n,wall}\rangle$; m for the radial coil width cw and depth cd and the excess radial gap; MA/m^2 for j_{coil}, m^3 for the volume of the coil winding packs Vol_{coils}, and m^2 for the first wall area $Area_{wall}$. The $\langle R\rangle$ values range from 6.2 m to 6.9 m, a factor of two smaller than for other stellarator reactors that have been studied. There is larger variation, a factor of 1.56, in $\langle p_{n,wall}\rangle$ (and hence in the area of the first wall, blanket, shield, and vacuum vessel wall) because of the different plasma aspect ratios. However, there is relatively little variation in the volume of the superconducting winding packs. The average on-axis magnetic field varies from 5 T to 6.5 T and the maximum field on the coils varies from 11 T to 15 T. All have a relatively thin radial depth for the winding pack, from 14 cm to 29 cm. The NCSX-1 case is chosen to illustrate parameters sensitivities in this paper because it should ultimately have a lower cost than the other cases due to its higher allowed value for $\langle p_{n,wall}\rangle$, at least for the LiPb/ferritic steel/He-cooled blanket/shield approach used here. Other blanket/shield approaches currently under study[5] could lead to a different optimization.

TABLE II. Compact Stellarator Reactor Parameters.

	NCSX-1	NCSX-2	MHH2-8	MHH2-16
$\langle p_{n,wall}\rangle$	3.33	2.67	2.13	2.4
$\langle R\rangle$, (m)	6.22	6.93	6.19	6.93
$\langle a\rangle$, (m)	1.38	1.54	2.29	1.85
$\langle B_{axis}\rangle$,(T)	6.48	5.98	5.04	5.46
B_{max}, (T)	12.65	10.9	14.9	15.2
j_{coil}	114	119	93	93
k_{max}	3.30	5.0	2.78	1.87
cw, (m)	0.598	0.719	0.791	0.502
cd, (m)	0.181	0.144	0.286	0.268
radial gap	0.026	0.012	0.007	0.005
□ (s)	0.88	1.04	1.46	1.25
Vol_{coils}	60.3	63.4	61.4	60.3
$Area_{wall}$	480	600	750	667

III. 1-D OPTIMIZATION

The 0-D optimization only determines global reactor parameters: $\langle R\rangle$, $\langle a\rangle$, $\langle B_{axis}\rangle$, $\langle p_{n,wall}\rangle$, □ and the coil

cross section. A 1-D power balance analysis is needed to determine the plasma parameters: the volume-average electron density $\langle n \rangle$, the density-averaged plasma temperature $\langle T \rangle$, $\langle \sigma v \rangle$, $P_{\text{radiation}}$, the operating point, and the startup path to ignition. A 1-D power balance code is used to study the effect of different plasma and confinement assumptions including density and temperature profiles, alpha-particle power losses, and helium particle confinement time for a given plasma and coil configuration.

Proper treatment of impurities is important in assessing reactor plasma performance. The electron density $n_e(r) = n_{DT}(r) + 2n_{He}(r) + \Sigma Z n_Z(r)$, so high impurity levels reduce $p_{\text{fusion}} \sim n_{DT}^2 \langle \sigma v \rangle$ through reduced n_{DT} and reduced electron temperature T_e (and hence the D-T temperature T_i) through higher radiative losses. Higher values of $\langle B_{\text{axis}} \rangle$, or confinement improvement factor H-ISS95, or $\langle R \rangle$ are needed to compensate for higher impurity levels. The impurities assumed in this study are carbon (Z = 6) and iron (Z = 26). Previous treatments[3,4] assumed that the impurity densities were a constant fraction of the electron density. However neoclassical treatment of impurity transport[10] gives $n_Z(r) = n_e(r) \times f_Z (n_e/n_{e0})^Z (T_e/T_{e0})^{-Z/5}$ where the impurity fractions $f_Z = n_Z/n_e$. The T_e ("temperature screening") term, which leads to an $n_Z(r)$ peaked off axis, is applicable when the main ion species (D-T) and the impurity ion are not both at high collisionality and so is probably applicable for the quasi-axisymmetric stellarator reactors of interest here. In addition, an $n_e(r)$ peaked off axis (hollow profile) leads to an $n_Z(r)$ peaked off axis as well. The Wendelstein 7-AS modular stellarator and the Large Helical Device have hollow $n_e(r)$ profiles with a center/peak density ratio of 0.8 at low collisionality. Hollow $n_e(r)$ and $n_Z(r)$ profiles are of interest because they can lead to enhanced impurity radiation to the wall near

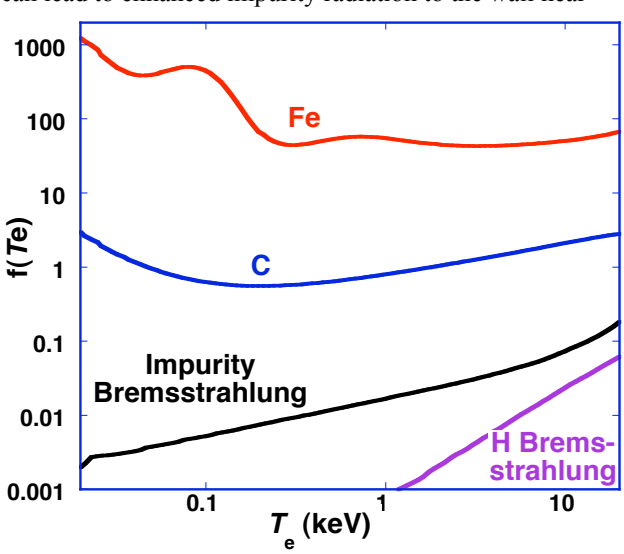

Fig. 6. Variation of radiative power with T_e.

the edge of the plasma, which reduces the thermal heat load on the divertor plates. The standard coronal model[11] for line radiation and electron-ion recombination is used for calculating the radiative power loss $p_{\text{radiation}} \sim n_e n_Z f(T_e)$ where $f(T_e)$ is plotted in Fig. 6.

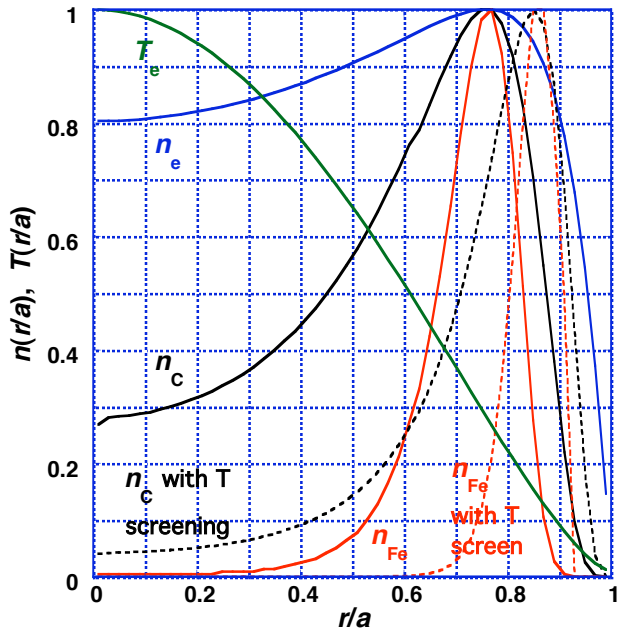

Fig. 7. Base density and temperature profiles.

The base radial profiles assumed are shown in Fig. 7: a hollow $n_e(r)$ with center/peak density ratio of 0.8, $T(r) \sim$ parabolic[1,5], and neoclassical impurity profiles $n_Z \sim n_e^Z$ with (dashed curves) and without (solid curves) the temperature screening term. The parameter assumptions used for this study are volume-average impurity fractions $\langle f_C \rangle$ = 1% and $\langle f_{Fe} \rangle$ = 0.01% without the temperature screening term for conservatism, $\tau_{He}^*/\tau_E = 6$ where τ_{He}^* is the net helium particle confinement time including recycling, and an alpha-particle energy loss fraction $f_{\alpha,\text{loss}} = 0.3$. The sensitivity of the results to the profile assumptions and parameter values has also been studied. The plasma energy confinement is characterized by the ISS-95 stellarator confinement scaling[13] $\tau_E^{\text{ISS-95}}$ =

$$0.26 P_{\text{heating}}^{-0.59} \langle n_e \rangle^{0.51} \langle B_{\text{axis}} \rangle^{0.83} \langle R \rangle^{0.65} \langle a \rangle^{2.21} \iota_{2/3}^{0.4}$$

where τ_E is in s, P in MW, n_e in 10^{20} m^{-3}, R and a in m, and $\iota_{2/3}$ is the rotational transform at $2/3a$. A confinement improvement factor H-ISS95 = $\tau_E/\tau_E^{\text{ISS-95}} < 5$ (twice present values) is used assuming improvements due to quasi-symmetry (very low effective ripple ε_{eff}) and further operating experience. Recent improvements[14] to the ISS-95 stellarator confinement scaling indicate H-ISS $\sim \varepsilon_{\text{eff}}^{-0.4}$, which suggests that large H-ISS factors should be possible for the low-ε_{eff} quasi-axisymmetric (tokamak-like) compact stellarators.

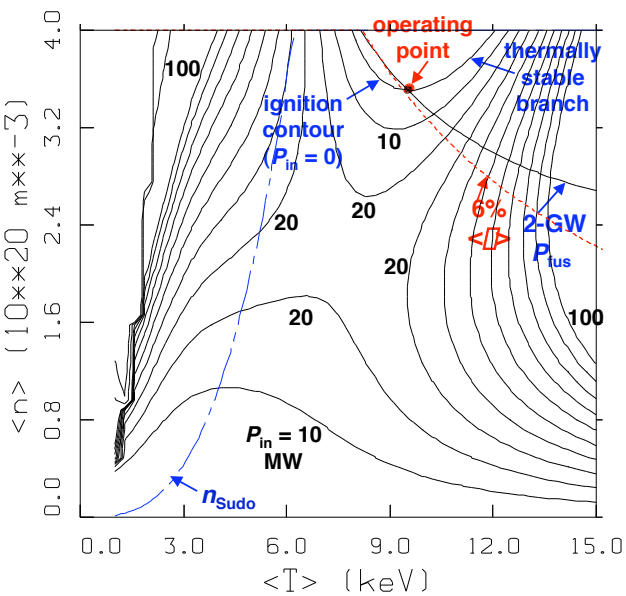

Fig. 8. Plasma operation contours for the base NCSX -1.

Figure 8 shows the results for an NCSX-1 case with $\langle R\rangle$ = 6.22 m and $\langle B_{axis}\rangle$ = 6.48 T, values obtained from the 0-D calculation summarized in Table II. The labeled contours indicate the heating power input required for a given point in the $\langle n\rangle$, $\langle T\rangle$ plane. The $\langle\beta\rangle$ = 6% and n_{Sudo} curves are also shown for reference; typically the maximum density values for good operation in stellarators are $\langle n\rangle$ = 1–2 x n_{Sudo} where n_{Sudo} is the density "limit" inferred from earlier experiments in Heliotron E[15]. The stepped left boundary corresponds to an assumed energy confinement time that rapidly decreases at $\langle n\rangle$ = 2 x n_{Sudo}. The operating point is the intersection of the 2-GW P_{fusion} curve with the thermally stable portion of the ignition contour (P_{in} = 0). The minimum power path to the operating point is through the saddle point, which requires ~22 MW of heating power. The operating point parameters are $\langle n\rangle$ = 3.5 x 10^{20} m^{-3}, $\langle T\rangle$ = 9.5 keV, $\langle\beta\rangle$ = 6.1%, $\langle f_{DT}\rangle$ = 83.8%, $\langle f_{He}\rangle$ = 4.9%, and Z_{eff} = 1.42. The minimum H-ISS95 value for a stable operating point is 4.15. Higher values for H-ISS95 lower the ignition contour, resulting in an operating point higher up the thermally stable (right) branch of the ignition contour. For the base NCSX-1 case with 30% of the alpha-particle power lost to the divertor, the total radiated power is 62 % of the power to the electrons and 46% of the total power to the plasma. Of the 128 MW of radiated power, most (79 MW) is hydrogenic bremsstrahlung with a smaller amount radiated by impurities (24.7 MW by carbon and 23.8 MW by iron). No beta limit is assumed in Fig. 8. The effect of imposing an energy confinement time that rapidly decreases close to $\langle\beta\rangle$ = 7.5% is to compress the heating contours at higher $\langle\beta\rangle$ (higher $\langle n\rangle$ and $\langle T\rangle$). The effect on the operating point is minor (less than 1% change in the plasma parameters), but the thermally stable branch of the ignition contour is much reduced and the ignition contour turns into a closed loop.

Table III summarizes the results for the four compact stellarator configurations using the base profiles and parameter assumptions. The values used for $\langle R\rangle$ and $\langle B_{axis}\rangle$ are taken from the highest $\langle p_{n,wall}\rangle$ cases for the 0-D scoping study results listed in Table II. The impurity and ~5% helium concentrations result in a Z_{eff} = 1.42. The minimum H-ISS95 values range from 3.8 to 4.2 and the $\langle\beta\rangle$ = 6.1%.

TABLE III. Base Plasma Parameters.

	NCSX-1	NCSX-2	MHH2-8	MHH2-16
$\langle R\rangle$, (m)	6.22	6.93	6.19	6.93
$\langle a\rangle$, (m)	1.38	1.54	2.29	1.85
$\langle B_{axis}\rangle$, (T)	6.48	5.98	5.04	5.46
H-ISS95	4.15	4.20	3.75	4.10
$\langle n\rangle$, 10^{20} m^{-3}	3.51	2.89	2.05	2.43
f_{DT}	0.841	0.837	0.837	0.839
f_{He}	0.049	0.051	0.051	0.050
$\langle T\rangle$, (keV)	9.52	9.89	9.92	9.74
$\langle\beta\rangle$, (%)	6.09	6.12	6.13	6.09

Table IV summarizes the differences in plasma parameters due to different assumptions for the plasma density and temperature profiles for the NCSX-1 case. The base case has a hollow density profile ($n \sim [1 - (r/a)^{12}][0.66 + (r/a)^2]$ for a center/peak density ratio of 0.8), a parabolic[1.5] temperature profile, and no temperature-screening factor in $n_Z(r)$. The "peaked n" case has the peak density on axis (0.66 replaced by 1.0) and the 0.1 $n_{pedestal}$ and 0.2 $n_{pedestal}$ cases have an edge density pedestal equal to 10% and 20% of the central density. The "T parabolic" and "T parabolic^2" cases have temperature profiles that are parabolic and parabolic-squared, and the 0.1 $T_{pedestal}$ and 0.2 $T_{pedestal}$ cases have an

TABLE IV. Effect of Profiles on Plasma Parameters.

Variation	$\langle n\rangle$ 10^{20} m^{-3}	$\langle T\rangle$ keV	H-ISS95	$\langle\beta\rangle$ %
Base case	3.51	9.52	4.15	6.09
Peaked n	3.36	9.85	4.00	6.03
0.1 $n_{pedestal}$	3.53	9.46	4.10	6.09
0.2 $n_{pedestal}$	3.57	9.34	4.05	6.09
T parabolic	3.23	10.82	4.40	6.36
T parabolic^2	3.60	9.01	4.00	5.92
0.1 $T_{pedestal}$	3.28	10.68	4.40	6.37
0.2 $T_{pedestal}$	3.22	11.11	4.50	6.50
Peaked n_Z	3.42	9.97	4.15	6.21
T screening	3.48	9.15	3.75	5.81

edge temperature pedestal equal to 10% and 20% of the central temperature. The "peaked n_Z" case has $n_Z \sim n_e$ (no n^Z term in n_Z). The "T screening" case includes the temperature-screening multiplying factor $T^{-Z/5}$ in n_Z. For the same P_{fusion}, the $\langle\beta\rangle$ values vary from 5.8% to 6.5%. The 0-D result assumed $\langle\beta\rangle$ = 6%. The difference is due to the profile effects illustrated in Table IV and the fact that $p_{fusion} \sim n_{DT}^2 \langle\sigma v\rangle$ is only approximately proportional to $\langle n\rangle^2 \langle T\rangle^2 \sim \langle\beta\rangle^2$, as illustrated by the difference shapes for the P_{fusion} = 2 GW and $\langle\beta\rangle$ = 6% curves in Fig. 8. The required minimum H-ISS95 varies from 3.75 to 4.5; the temperature pedestals and temperature screening of impurities have the largest impact. The variation in $\langle T\rangle$ (from 9 keV to 11.1 keV) is larger than the variation in $\langle n\rangle$ (from 3.2 to 3.6 x 10^{20} m^{-3}).

Fig. 9 illustrates the sensitivity of the H-ISS95 and $\langle\beta\rangle$ values to τ_{He}^*/τ_E for the NCSX-1 configuration where the base case has τ_{He}^*/τ_E = 6. The variation of H-ISS95 with τ_{He}^*/τ_E is due to the increase in f_{He} (from 2.5% to 10.2%) and the resulting decrease in f_{DT} (from 88.8% to 73.5% and f_{DT}^2, which enters in P_{fusion}, from 0.79 to 0.54) as τ_{He}^*/τ_E varies from 3 to 12. The large change in the $\langle\beta\rangle$ value is due to the same effect. In this case the variation in $\langle n\rangle$ (from 3.1 to 4.3 x 10^{20} m^{-3} is larger than the variation in $\langle T\rangle$ (from 9.61 keV to 9.95 keV). Fig. 10 illustrates the sensitivity of the H-ISS95 and $\langle\beta\rangle$ values to $f_{\alpha,loss}$, the fraction of the alpha-particle power that is lost. The main benefit in reducing the alpha-particle power lost from a power balance viewpoint is a reduction in the H-ISS95 required, from 4.15 to 3.15. A more important reason is to reduce the energetic alpha-particle flux to the divertor plates. There is almost no change in the $\langle\beta\rangle$ values in this case and relatively small changes in $\langle n\rangle$ (from 3.82 to 3.51 x 10^{20} m^{-3}) and $\langle T\rangle$ (from 9.52 keV to 8.57 keV) as $f_{\alpha,loss}$ increases from 0 to 0.3.

IV. SUMMARY

Four quasi-axisymmetric compact stellarators with different plasma and coil configurations were analyzed for their potential as ignited reactors without the current drive and disruption issues of tokamaks. Determination of the optimum reactor parameters involved both the plasma and coil geometry and the reactor constraints. A 0-D (volume-average) approach for optimizing the main reactor parameters employed dimensionless parameters that characterize the plasma and coil configurations. For each coil configuration a given average neutron wall loading uniquely determined $\langle R\rangle$ through the $A_{surf}/\langle R\rangle^2$ parameter. Fixing the allowable value for $\langle\beta\rangle$ determined the value of $\langle B_{axis}\rangle$. The results were constrained by the requirements that there be adequate distance between the edge of the plasma and the center of the nonplanar coils

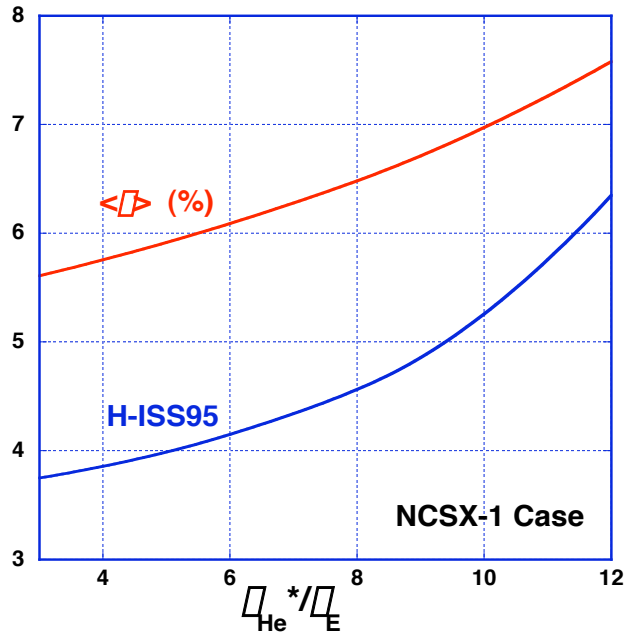

Fig. 9. Plasma parameter sensitivity to τ_{He}^*/τ_E.

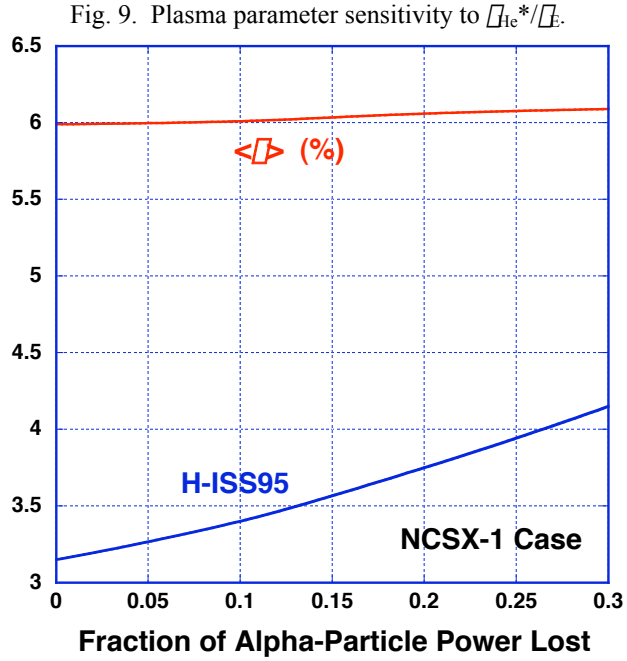

Fig. 10. Plasma parameter sensitivity to alpha-particle power lost.

and that j_{coil} not exceed the current density limit for the low-T_c superconductor. The four cases led to stellarator reactors with $\langle R\rangle$ = 6-7 m, a factor 2–3 smaller than in previous stellarator reactor studies and closer to tokamaks in size. The NCSX-1 case was chosen to illustrate parameter sensitivities because it should ultimately have a lower cost than the other cases due to its higher allowed value for $\langle p_{n,wall}\rangle$, at least for the LiPb/ferritic steel/He-cooled blanket/shield approach analyzed so far.

A 1-D power balance analysis was used to determine the plasma parameters for the ignited operating point and to study the sensitivity to different plasma profile assumptions and parameter values. The base radial profiles assumed were a hollow $n_e(r)$ with center/peak density ratio of 0.8, $T(r) \sim$ parabolic$^{1.5}$, and neoclassical impurity profiles $n_Z \sim n_e^Z$ without the temperature screening term. The minimum-power path to a stable operating point requires ~22 MW of heating power and a minimum H-ISS95 = 4.15. The operating point parameters were $\langle n \rangle = 3.5 \times 10^{20}$ m^{-3}, $\langle T \rangle = 9.5$ keV, $\langle \beta \rangle = 6.1\%$, $\langle f_{DT} \rangle = 83.8\%$, $\langle f_{He} \rangle = 4.9\%$, and $Z_{eff} = 1.42$. For the base NCSX-1 case with 30% of the alpha-particle power lost to the divertor, the total radiated power was 62 % of the power to the electrons and 46% of the total power to the plasma. Practical coil configurations need to be developed for some newer plasma configurations that have alpha-particle energy losses in the 5-10% range. In addition the assumed plasma temperature profiles were not consistent with high edge radiation losses and need to be calculated self-consistently, which is done in the full systems/optimization code.

A major issue that is beyond the scope of the 0-D optimization and the 1-D power balance calculation of the plasma parameters discussed in this paper is the type of divertor that would be used for particle and power handling in a reactor. It would most likely be based on the divertor concepts being developed in the Wendelstein 7-X, but this is an area of on-going study. The power load to the divertor can be reduced by decreasing the alpha-particle energy loss fraction and increasing the power radiated to the wall. An alpha-particle energy loss fraction $f_{\alpha,loss} = 0.3$ was used for this study. While this is not a problem for the overall power balance, compact stellarator configurations with a lower $f_{\alpha,loss}$ are needed. Some configurations with $f_{\alpha,loss} < 0.1$ have been developed[12] but not yet optimized with respect to the coil geometry. Tailoring the edge electron temperature and impurity profiles is being studied to create a high edge radiating layer as was done in Tore Supra.

ACKNOWLEDGMENTS

This research was supported by USDOE under Contract DE-AC05-00OR22725 with UT-Battelle, LLC.

REFERENCES

[1] J.F. LYON et al., "Compact Stellarators as Reactors," 18th Fusion Energy Conference, Sorrento 2000.

[2] C.D. BEIDLER et al, "Recent Developments in Helias Reactor Studies," Proceedings of 13th International Stellarator Workshop, Canberra, Australia (February 2002).

[3] R. MILLER and the SPPS Team, "The Stellarator Power Plant Study," University of San Diego Report UCSD-ENG-004 (1996).

[4] J.F. LYON et al., Plasma Physics and Controlled Nuclear Fusion Research 1994, Seville 1994, Vol. 2., 655 (IAEA Vienna 1985); also J.F. LYON et al., *Fusion Engineering and Design* **25**, 85 (1994).

[5] L. EL-GUEBALY, A.R. RAFFRAY, S. MALANG, J.F. LYON, L.P. KU, and the ARIES Team, "Benefits of Radial Build Minimization and Requirements Imposed on ARIES Compact Stellarator Design," These proceedings.

[6] G.H. NEILSON, M.C. ZARNSTORFF, J.F. LYON, and the NCSX Team, "Physics Design of the National Compact Stellarator Experiment," *J. Plasma and Fusion Research* **78**, 214 (2002).

[7] P. GARABEDIAN, L.P. KU, and the ARIES Team, "Physics Basis for the ARIES-CS Compact Stellarator Reactor," These proceedings.

[8] G.H. NEILSON et al., *Phys. Plasmas* **7**, 1911 (2000).

[9] L. EL-GUELBALY, private communication, (2004).

[10] S.P. HIRSHMAN and D.J. SIGMAR, *Nuclear Fusion* **21**, 1079 (1981).

[11] H.P. SUMMERS and R.W.P. McWHIRTER, *J. Phys. B* **12**, 1979 (1979).

[12] L.P. KU, "Progress in Configuration Development for Compact Stellarator Reactors," ARIES Project Meeting, Madison, June 2004.

[13] U. STROTH et al., *Nuclear Fusion* **39**, 11 (1996).

[14] H. YAMADA et al, "Study on Energy Confinement Time of Net-Current Free Toroidal Plasmas Based on Extended International Stellarator Database," 31st EPS Conference on Plasma Phys. London, June 2004, ECA Vol.**28B**, P-5.099 (2004).

[15] S. SUDO et al., *Nuclear Fusion* **30**, 11 (1990).